

Adsorption of gallic acid by tailor-made magnetic metal-ceramic nanocomposites

Original

Adsorption of gallic acid by tailor-made magnetic metal-ceramic nanocomposites / Pirozzi, D.; Pansini, M.; Marocco, A.; Esposito, S.; Barrera, G.; Tiberto, P.; Allia, P.; Sannino, F.. - In: JOURNAL OF MOLECULAR LIQUIDS. - ISSN 0167-7322. - ELETTRONICO. - 371:(2023), p. 121083. [10.1016/j.molliq.2022.121083]

Availability:

This version is available at: 11583/2974604 since: 2023-01-13T14:59:38Z

Publisher:

ELSEVIER

Published

DOI:10.1016/j.molliq.2022.121083

Terms of use:

This article is made available under terms and conditions as specified in the corresponding bibliographic description in the repository

Publisher copyright

Elsevier postprint/Author's Accepted Manuscript

© 2023. This manuscript version is made available under the CC-BY-NC-ND 4.0 license
<http://creativecommons.org/licenses/by-nc-nd/4.0/>. The final authenticated version is available online at:
<http://dx.doi.org/10.1016/j.molliq.2022.121083>

(Article begins on next page)

36 **ABSTRACT**

37

38 In the last years gallic acid (GA) has been used in a growing number of industrial
39 applications, thanks to its interesting properties. Unfortunately, the consequent presence
40 of GA in wastewaters raises significant environmental problems. In this view, two
41 tailor-made magnetic metal-ceramic nanocomposites, obtained from zeolite A, were
42 developed for the adsorptive separation of GA from wastewaters. Optimized
43 configurations of the nanocomposites, to increase their adsorption capacity and stability,
44 were obtained by suitable modification of a patented process.

45 The adsorption process was characterized as regards the role played by the most
46 relevant parameters (kinetics, pH, GA concentration). The GA removal was strongly
47 affected by pH. The experimental results suggested the interactions between GA and the
48 nanocomposites to be based on two different mechanisms.

49 The adsorption kinetics were in all cases described by the pseudo second-order
50 model. The adsorption isotherms data were satisfactorily described by the Sips model, a
51 combination of the Langmuir and Freundlich isotherm type models.

52 Suitable conditions were found to achieve the GA desorption, as well as the
53 recycle of the magnetic adsorbents. In this view, a procedure for the thermal
54 regeneration of the exhausted adsorbent was developed on the basis of the TG and DTA
55 analyses. In order to offer a more environmentally friendly approach, as well as to
56 achieve a full recovery of the economically valuable GA, a procedure for the alkaline
57 desorption was successfully developed.

58

59 *Keywords: magnetic metal ceramic nanocomposites, gallic acid, adsorption,*
60 *sustainable regeneration.*

61

62

63

64

65

66

67

68 1. Introduction

69

70 In the last years, the Gallic Acid (GA), 3,4,5-trihydroxybenzoic acid, has been
71 increasingly used in the pharmaceutical industry due to its antioxidant, anti-
72 inflammatory, antibacterial, neuroprotective and antitumor properties (Lu et al., 2006;
73 Al Zahrani et al., 2020). It has also been used for food preservation (Zheng et al., 2018)
74 due to its ability to reduce the rancidity, and for anti-corrosion protection of steel
75 surfaces (Badhani et al., 2015). Furthermore, its ability to bind proteins has been
76 exploited to develop innovative surfaces for sensing and catalysis (Sousa et al., 2018).
77 Moreover, GA was used in conjugation with solid materials to improve its native
78 properties: for example, with chitosan to improve its antioxidant ability (Pasanphan et
79 al., 2010), with gold nanoparticles (Moreno-Alvarez et al., 2010) or with PVA
80 composites (Yang et al., 2021), to enhance its antibacterial activity.

81 In spite of its interesting properties, the presence of GA in wastewater is
82 associated with significant environmental problems. First of all, GA affects the color
83 and the smell of water. Secondly, GA may react with chlorine, widely used as for
84 water disinfection, forming compounds such as chloroform and haloacetic acids. These
85 compounds can reduce the oxygen dissolved in watercourses, which is essential for the
86 survival of aquatic organisms, and are toxic for humans, being carcinogenic,
87 teratogenic, and mutagenic (Zhang et al., 2015). In addition, it has been shown that GA
88 may cause hemorrhagic liposis of cerebral muscles and intracerebral hemorrhage (Hsieh
89 et al., 2015). Many valuable studies suggest adsorption as a method for separation of
90 organic matter from water, owing to its efficiency, intrinsic simplicity and low cost
91 (Srivastava et al., 2009; Addorisio et al., 2010; Sannino et al., 2012; Sannino et al.,
92 2013; Esposito et al., 2013). The adsorption offers a simple, cheap and efficient method
93 to separate the polyphenols from the complex aqueous solutions (Addorisio et al., 2011;
94 Pirozzi et al., 2014). So far, activated carbon, silica gel, polymeric and macroporous
95 resins have been proposed as sorbents for phenolic compounds. However, adsorption
96 processes may be operated or by columnar plants or in batch reactor systems under
97 continuous stirring and both systems exhibit serious drawbacks strongly hindering their
98 diffusion. Actually, columnar plants are subject to flow troubles arising from the
99 necessity of avoid channeling (occurring at low package density of the adsorbent) and

100 high head losses (occurring at high package density of the adsorbent), whereas batch
101 reactor systems suffer from the difficulty arising in the separation of the adsorbent, if it
102 is a loose powder, from the liquid. Furthermore, also the regeneration of the exhausted
103 adsorbent often is not easy and straightforward (Di Martino et al., 2015). In order to
104 establish these issues, we have developed magnetic metal-ceramic nano-composite
105 adsorbents, to allow a simple separation from the liquid phase by an external magnet,
106 thus preventing the generation of contaminants such as flocculants, and making easier
107 the reuse of the adsorbent and the disposal of the waste. To this scope, tailor-made
108 nanocomposites have been produced. Zeolite precursor have been adopted, to exploit
109 peculiar properties of zeolites, such as high cation exchange capacity, swelling, and
110 wide availability. The magnetic nano-composite adsorbents have been obtained by
111 suitable modification of a patented process (Esposito et al., 2015; Esposito et al., 2018;
112 Pansini et al., 2018) following a two-step procedure. First, commercial zeolites were
113 exchanged with Fe^{2+} ions. Subsequently, the heavy-metal cation-exchanged zeolites
114 underwent a thermal treatment at relatively mild temperatures (500-900 °C range) under
115 a reducing atmosphere (2.0 vol.% H_2 in Ar). After the thermal treatment, the original
116 zeolite structure was almost totally destroyed to obtain a dispersion of metallic Fe^0
117 nanoparticles in a mostly amorphous matrix of silica and alumina. Consequently, the
118 physical-chemical properties of the nanocomposite were significantly different from
119 those of the parent zeolite. Yet, the nanocomposite exhibited a residual porosity
120 (Esposito et al., 2018), which is a remnant of the parent zeolite structure, that may have
121 an impact on its applications as adsorbent. In addition, the silanol groups of the
122 nanocomposites, also a remnant of the parent zeolite, may act as Bronsted sites,
123 ensuring favourable interactions for adsorption processes. The proposed procedure of
124 production of magnetic nanocomposites is very simple and cheap, and easily scalable.
125 Similar nanocomposites have so far been tested in biochemical and environmental
126 applications (Pansini et al., 2018; Marocco et al., 2019; Pansini et al., 2017; Esposito et
127 al., 2020; Sannino et al., 2022) and as moon dust simulat (Freyria et al., 2019; Manzoli
128 et al., 2021), showing a large potential for further applications. A commercial zeolite A,
129 well known as regards its features, has been selected as starting material for its high
130 cation exchange capacity, due to the Si/Al ratio = 1.00, and for its low cost, due to the
131 large availability. Although various magnetic composites have been previously

132 synthesized providing a magnetite core to an adsorbent material, employing iron sludge
133 (Wan et al., 2020) or by modification of activated carbon (Guo et al., 2018), no
134 magnetic materials have been so far obtained by exchange of Fe^{2+} ions. This study aims
135 at evaluating the ability of the magnetic nanocomposites in the removal of GA from
136 wastewaters by adsorption, investigating the most relevant physicochemical aspects of
137 the GA adsorption, with particular attention to the main process parameters (solid/liquid
138 ratio, pH, time, initial concentration of GA). A regeneration procedure for the exhausted
139 adsorbent has also been proposed, to ensure the reuse of the magnetic nanoparticles, as
140 well as the recovery of the GA, which is of interest due to its significant commercial
141 value.

142

143 **2. Materials and Methods**

144

145 *2.1. Materials*

146

147 Carlo Erba reagent grade synthetic zeolite 4A ($\text{Na}_{12}\text{Al}_{12}\text{Si}_{12}\text{O}_{48}\cdot 27\text{H}_2\text{O}$,
148 framework type LTA, was used in this study. ~~The average grain size is about 8-10 μm . Its~~
149 ~~grain size distribution is reported in~~ (Marocco et al., 2011). Exchange solutions were
150 prepared dissolving Carlo Erba reagent grade 99.5 wt.% $\text{FeSO}_4\cdot 7\text{H}_2\text{O}$ and NH_4Cl in
151 doubly distilled water. Gallic acid (3,4,5-trihydroxybenzoic acid, 98.0% purity),
152 employed as a bioactive compound, was supplied by Fluka (Bruch, Switzerland).

153

154 *2.2. Preparation of Gallic Acid solution*

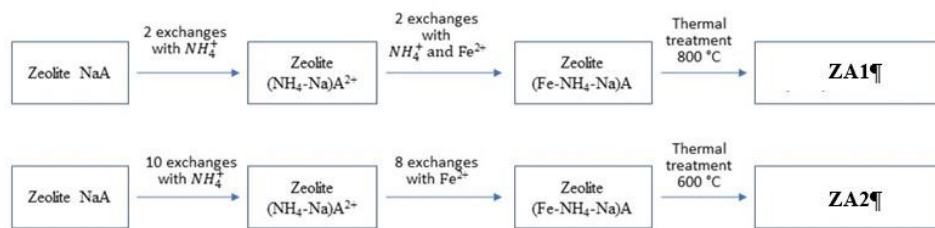
155

156 GA (25 mg) was dissolved in 10 mL of ultrapure water for 2 h at room
157 temperature under magnetic stirring to obtain a 15 mM solution. It was stored at 4 °C in
158 the dark to avoid oxidation reactions. The stock solution was suitably diluted with
159 ultrapure water to have the following concentrations: 1000, 800, 500, 250, 150, 50 and
160 10 μM . The analytical determination of GA was carried out by UV-vis
161 spectrophotometer (ThermoScientific Varioskan Flash, Finland) at 265 nm.

162

163 *2.3. Preparation of metal ceramic nanocomposites*

164 Two magnetic metal-ceramic nanocomposites were prepared starting from zeolite
 165 A: ZA1 (labeled as (Fe,H)A800C-0min in previous works (Pansini et al., 2018); ZA2
 166 (labeled as (Fe,H)A600C-90min in previous works (Pansini et al., 2018). In Figure 1 the
 167 procedure followed in preparing the metal-ceramic nanocomposites is outlined.
 168



169 **Figure 1.** Procedure followed in the preparation of ZA1 and ZA2 magnetic adsorbents.
 170

171
 172 The magnetic nanocomposite ZA1 was produced as follows. Zeolite A was contacted
 173 with a $[\text{NH}_4^+] = 0.1 \text{ M}$ solution at a wt. solid/liquid ratio of $(\text{S/L}) = 1/50 \text{ g/g}$, room
 174 temperature and contact time $(t) = 1 \text{ h}$. Then, the solid was separated from the liquid
 175 through filtration and contacted again with a fresh solution. This operation was iterated
 176 two times. Subsequently, this sample of NH_4^+ -exchanged zeolite A was contacted with a
 177 $[\text{Fe}^{2+}] = [\text{NH}_4^+] = 0.1 \text{ M}$ solution at a wt. solid/liquid ratio of $(\text{S/L}) = 1/50$ and contact
 178 time $(t) = 1 \text{ h}$. In this exchange the temperature (T) was $\approx 7 \text{ }^\circ\text{C}$ and Ar was bubbled
 179 through the solution to prevent Fe^{2+} oxidation (Weidentaler et al., 2005). The solid
 180 particles were separated from the liquid through filtration and contacted again with a
 181 fresh solution. This operation was iterated two times. The resulting powders were
 182 washed with doubly distilled water, dried for about one day at $80 \text{ }^\circ\text{C}$, and stored for at
 183 least 3 days in an environment with about 50% relative humidity, to allow water
 184 saturation of the zeolite. This sample of NH_4^+ and Fe^{2+} exchanged zeolite A was
 185 subjected to the following thermal treatment under a reducing atmosphere (created by a
 186 flow of a H_2 -Ar gaseous mixture, containing 2 vol. % H_2) in an Al_2O_3 tubular furnace
 187 (inner diameter = 6.9 cm, height = 91 cm), using Pt crucibles: heating from room
 188 temperature up to $800 \text{ }^\circ\text{C}$ (15 $^\circ\text{C}/\text{min}$ heating rate); as soon as the temperature of $800 \text{ }^\circ\text{C}$
 189 was reached, the heating system of the furnace was switched off and the sample was left
 190 to cool down to room temperature within the furnace. The sample ZA2 was produced as

191 follows. Zeolite A was contacted with a $[\text{NH}_4^+] = 0.1 \text{ M}$ solution according to the same
192 procedures of the previous sample. This exchange was iterated ten times. Then this
193 sample of NH_4^+ exchanged zeolite A was contacted with a $[\text{Fe}^{2+}] = 0.1 \text{ M}$ solution at a
194 wt. solid/liquid ratio of $(\text{S/L}) = 1/50 \text{ g/g}$, temperature $(\text{T}) \approx 7 \text{ }^\circ\text{C}$, contact time $(\text{t}) = 1 \text{ h}$
195 and under Ar bubbling. This operation was iterated eight times. The resulting powders
196 were washed, dried and kept as in the previous case. This sample of NH_4^+ and Fe^{2+}
197 exchanged zeolite A was subjected to the following thermal treatment under a reducing
198 atmosphere: heating from room temperature up to $600 \text{ }^\circ\text{C}$ ($15 \text{ }^\circ\text{C}/\text{min}$ heating rate) and
199 subsequent thermal treatment at $600 \text{ }^\circ\text{C}$ for 90 min; then, the heating system of the
200 furnace was switched off and the sample was left to cool down to room temperature
201 within the furnace. Samples ZA1 and ZA2 were subjected to X-ray characterization
202 according to what reported in Clayden et al., 2003.

203

204 2.4. Characteristics of the nanocomposites

205

206 The Fe^{2+} and NH_4^+ exchanged zeolite A undergoes the following phenomena
207 during the thermal treatments under the reducing atmosphere (Colantuono et al., 1997):

208 1) Shrinkage by dehydration;

209 2) Evolution of gaseous NH_3 , thus leaving hydrogen ions to balance the negative
210 charges of the zeolitic structure, with the formation of acidic Lewis sites;

211 3) Reduction to Fe^0 or to Fe_3O_4 (with a possible structural damage of the zeolite
212 framework);

213 4) Migration of the newly formed Fe^0 atoms or Fe_3O_4 particles to form clusters
214 located within the microporous cavities of the zeolite;

215 5) Migration of the newly formed Fe^0 atoms or Fe_3O_4 particles outside the zeolite
216 cavities to form metallic aggregates at the outer surface of the zeolite grains;

217 6) Thermal collapse of the zeolite framework;

218 7) Possible formation of amorphous and other crystalline phases.

219 The *raison d'être* of the modalities of preparation of the two nanocomposites,
220 clearly explained in detail in ref. (Pansini et al., 2018), are summarized hereafter.
221 Sample ZA1 exhibits a large amount of acidic Lewis sites very useful in adsorption
222 processes and a moderate magnetic response sufficient to perform a magnetic separation

223 of the solid from the liquid (saturation magnetization $M_s = 4.2$ emu/g) (Pansini et al.,
224 2018). Sample ZA2 exhibits a strong magnetic response (saturation magnetization $M_s =$
225 12.3 emu/g), far more than sufficient to perform a magnetic separation of the solid from
226 the liquid, and a moderate amount of acidic Lewis sites (Pansini et al., 2018). Moreover,
227 a complete chemical, mineralogical, physical characterization of samples ZA1 and ZA2
228 can be found in the same ref. (Pansini et al., 2018).

229

230 2.5. Adsorption experiments

231

232 Batch experiments of GA adsorption by magnetic nanocomposites were
233 performed by investigating the following experimental conditions:

234 • pH. To evaluate the effect of pH, GA adsorption experiments were carried out at
235 solid/liquid (s/l) ratio of 1/100. Actually, 20 mg of adsorbent were contacted with 2 mL
236 of 150 $\mu\text{mol/L}$ GA solution (obtained by diluting 15 mmol/L stock solution) for 2 h, at
237 pH between 3.0 and 8.0. The pH of the solution was properly controlled by addition of
238 either 0.01 or 0.10 mmol/L HCl or NaOH solution. After incubation in a rotatory shaker
239 at 25 °C, the magnetic adsorbents were separated from the liquid using an external
240 magnet (VA03, UNIDISP s.r.l. Italy) and the liquid was analysed to evaluate GA
241 concentration by spectrophotometric analysis. The amount of adsorbed GA was
242 calculated as the difference between the GA quantity initially added and that present in
243 the liquid at equilibrium. Blanks of GA in ultrapure water were analysed in order to
244 check for phenolic compound stability and/or adsorption on the vials.

245 • Kinetic tests. To evaluate the effect of time on GA adsorption, experiments were
246 performed at solid/liquid ratio 1/100, contacting 20 mg of adsorbent with 2 mL of 150
247 $\mu\text{mol/L}$ GA solution at pH 5.0 (pH of maximum adsorption). The suspensions were
248 stirred for 0.5, 1.0, 2.0, 3.0, 4.0, 6.0, 24 and 48 h. The longest contact times was that
249 needed to attain equilibrium.

250 • Adsorption isotherm. The adsorption isotherms were obtained by contacting 20
251 mg of adsorbent with 2 mL (s/l = 1/100) of GA solution with concentration ranging
252 between 0.01–1000 $\mu\text{mol/L}$. The pH was kept constant at 5.0 (pH of maximum
253 adsorption) by addition of 0.10 or 0.01 mol/L HCl or NaOH aqueous solution. The

254 samples were incubated for 24 h (time sufficient to attain equilibrium) and successively
255 subjected to the separation procedure previously described.

256

257 2.6 Desorption experiments

258

259 The desorption experiments were carried out as follows. 20 mg of adsorbent were
260 contacted with 2 mL ($s/l = 1/100$) of 200 and 1000 $\mu\text{mol/L}$ GA solution for 24 h, at pH
261 5.0. Immediately after the end of this GA adsorption step, the solid was separated from
262 the liquid, by using the external magnet, as previously described. Then, the exhausted,
263 GA bearing, adsorbent was contacted with 2 mL of ultrapure water at two different pH
264 values (5.0 and 8.0). After shaking this suspension at 25 °C for 24 h, the adsorbent was
265 magnetically separated from the liquid, and the concentration of the released GA therein
266 was determined.

267 For each magnetic adsorbent, two desorption cycles were carried out, performing
268 each re-adsorption stage with GA at the same initial concentration (200 and 1000
269 $\mu\text{mol/L}$) and at pH 5.0. The concentration of released GA was determined after each
270 desorption stage.

271

272 2.7 Thermal analysis

273

274 GA was subjected to simultaneous differential thermal analysis (DTA) and
275 thermogravimetric analysis (TG) under inert atmosphere (N_2), using a Perkin-Elmer
276 thermo-analyzer STA 6000, with Al_2O_3 as reference material. The TG and DTA tests
277 were performed keeping 9.00 mg of GA under nitrogen atmosphere, varying the
278 temperature from 30 to 900 °C. A heating rate of 10 °C min^{-1} was adopted.

279

280 2.8 FTIR analysis

281

282 Fourier transform infrared spectroscopy (FT-IR) spectra were recorded using a
283 Jasco FT-IR 430 spectrophotometer (Jasco Europe, Cremella, Italy). GA, ZA1, ZA2,
284 and GA-complexes, obtained by adsorption of each magnetic adsorbent with GA
285 solution at 1000 $\mu\text{mol/L}$ initial concentration, at pH 5.0 for 24 h at 25 °C, were dried

286 and ground into a powder form before the FT-IR analyses. Sample powders were mixed
287 in a 1:100 weight ratio with KBr and pressed into a disk under vacuum. The samples
288 were scanned from 400 cm^{-1} to 4,000 cm^{-1} .

289

290 **3. Results and discussion**

291

292 *3.1. IR Spectra*

293

294 In order to verify the effective adsorption of GA on the magnetic adsorbents, IR spectra
295 of both the pure GA and the exhausted nanocomposite after GA adsorption were
296 obtained, as shown in the Fig. 2.

297 The IR spectrum of pure GA shows a shoulder at 3492 cm^{-1} due to the free
298 phenolic O-H stretching and the two bands in the range 3367-3290 attributable to acidic
299 O-H stretching. As expected, the presence of carbonyl group of C=O stretching
300 vibrations is evidenced by the observation of the band at 1703 cm^{-1} , whereas the band at
301 1618 cm^{-1} appears related to C=C stretching vibration of the aromatic ring, and the band
302 at 791 cm^{-1} can be attributed to δ_{cc} benzene ring vibration. Moreover, as reported in
303 literature, the aromatic ring shows two bands at 1541 and 1450 cm^{-1} (Hirun et al., 2012).

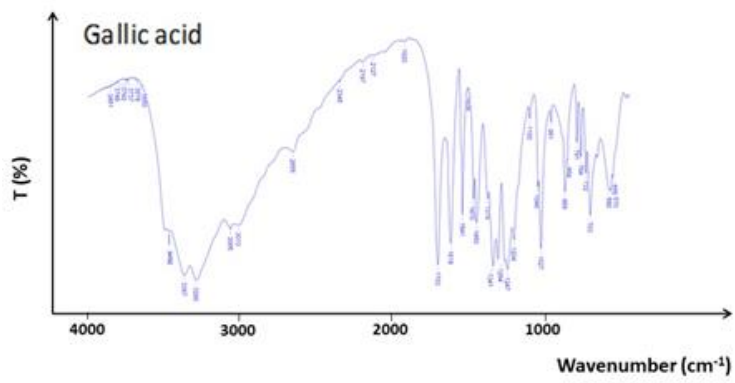
304 The spectra of the exhausted nanocomposites after GA adsorption are composed
305 of combined bands of both GA and each magnetic nanocomposite, demonstrating the
306 presence of adsorbed GA of the surface of nanocomposites. The evidence of this claim
307 is the shift of 3435 cm^{-1} band present in ZA1 to the intense peak at 3413 cm^{-1} observed
308 in the GA-ZA1 nanocomposite on account of the presence of GA. Unlike ZA1
309 nanocomposite, the shift of the band at 3435 cm^{-1} is not observed in the FTIR spectra of
310 ZA2 and GA-ZA2 nanocomposites. Thus, GA adsorption is denoted solely by the slight
311 increase of the intensity of the peak recorded in the GA-ZA2 spectrum with respect to
312 ZA2 spectrum. This item appears perfectly consistent with the lower amount of GA
313 adsorbed by ZA2 than ZA1 adsorbent (*vide infra*).

314

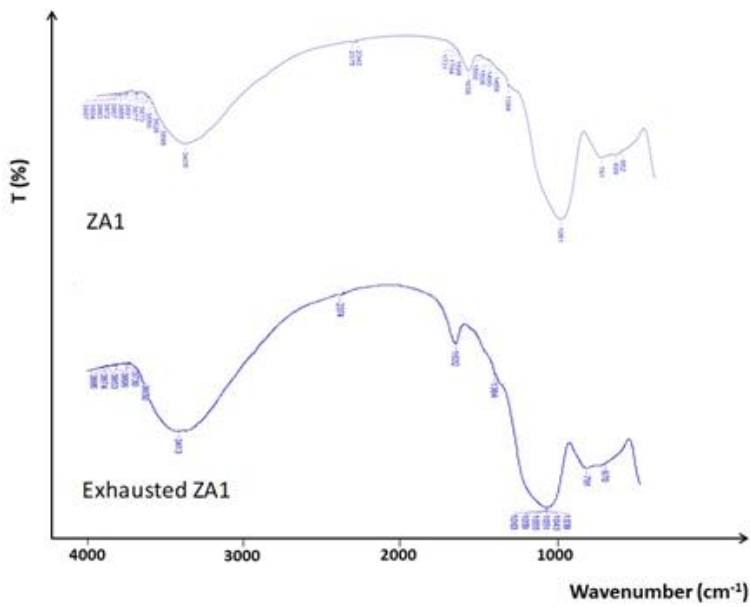
315

316

317



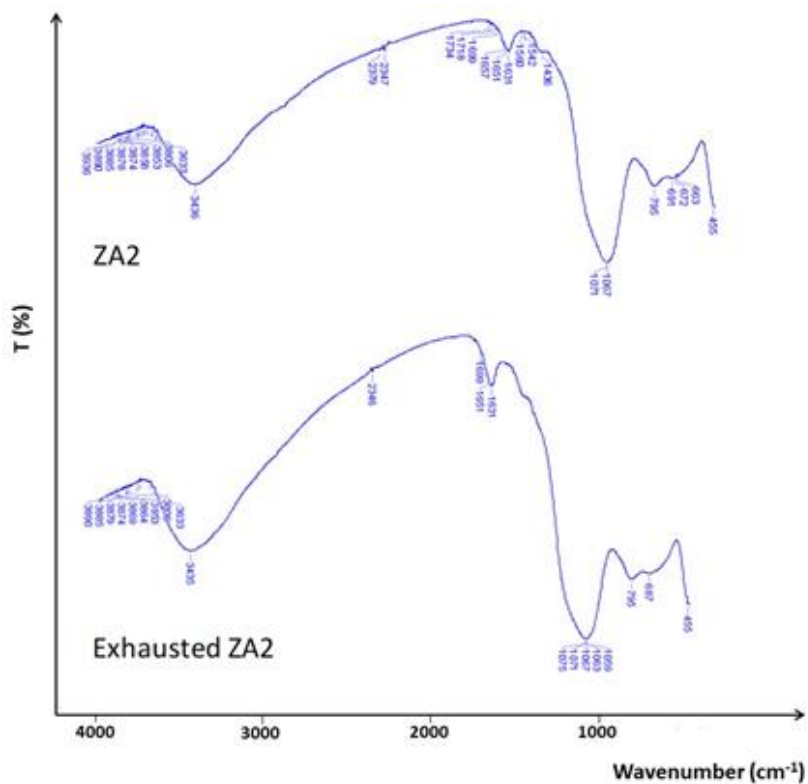
a)



b)

318
319

320
321



c)

322
323

324 **Figure 2.** Room-temperature FTIR spectra of (a) pure gallic acid, (b) ZA1 and
325 exhausted ZA1 obtained after gallic acid adsorption, and (c) ZA2 and exhausted ZA2
326 obtained after gallic acid adsorption.

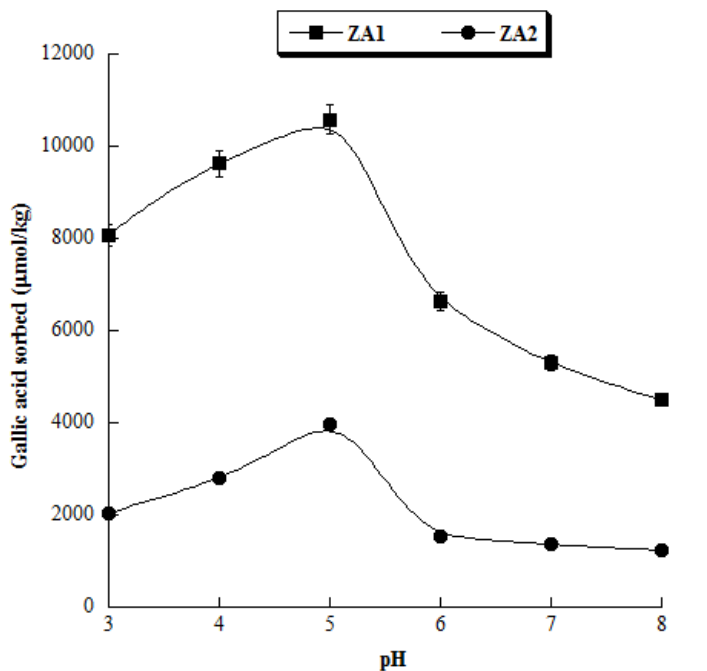
327

328 *3.2. Effect of pH on GA adsorption*

329

330 A set of experiments was carried out to characterize the effect of pH on the
331 adsorption of GA using both the magnetic nanocomposites ZA1 and ZA2. It has been
332 previously shown (Friedman and Jurgens, 2000) that the pH of the medium, as well as
333 the presence of metal ions, may significantly affect the stability and the electronic
334 absorption spectra of polyphenols. As a matter of facts, the pH of the solution may
335 affect not only the surface properties of the adsorbents but also the ionization state of

336 the adsorbate. The Figure 3 reports the amount of gallic acid adsorbed on the
337 nanocomposites ZA1 and ZA2 as a function of the pH.
338



339
340 **Figure 3.** Effect of pH on the adsorption of gallic acid on the magnetic adsorbents ZA1
341 and ZA2. S/L ratio = 1/100, initial gallic acid concentration = 150 µmol/L, contact time
342 = 2h

343
344 Both curves show an adsorption maximum at pH close to 5. The adsorbed
345 amounts of GA are higher in the case of ZA1 (about 10,500 µmol/kg) and lower in the
346 case of ZA2 (about 4,000 µmol/kg). Significant changes in GA uptake were observed
347 when adopting pH values different from the optimum. For both materials, the
348 adsorption of GA significantly increases with increasing pH from 3.0 to 5.0, then it
349 decreases at pH > 5.0, tending towards a horizontal asymptote at pH values higher than
350 6.0. Consequently, all the subsequent experiments of GA adsorption were carried out at
351 pH=5, corresponding to the maximum adsorption.

352 In order to explain these results, it is worth observing that the points of zero-
353 charges of ZA1 and ZA2, calculated from ζ -potential curves (Pansini et al., 2018), are
354 5.6 and 3.7 respectively. As a consequence, when the pH is at the optimum conditions
355 (i.e. close to 5.0), the surface charge of magnetic nanocomposites is close to neutrality.

356 On the other hand, it is known that GA is a weak polyprotic acid with four acidic
357 protons (the carboxylic group and three phenolic groups), undergoing a pH-dependent
358 deprotonation. Consequently, the distribution between GA and the different gallate
359 anions is affected by the medium pH in a complex way (Jabbari, 2015; Pant et al.,
360 2019). The deprotonation state of GA at a given pH can be expressed in terms of the
361 degree of deprotonation, i.e. the ratio between acidic donated H^+ and total acidic H^+ .
362 When the pH is close to 5.0 the degree of deprotonation ratio is about 0.25 (Pant et al.,
363 2018), thus indicating that GA molecules are still mostly protonated (i.e. uncharged).

364 A similar conclusion can be drawn considering the zero-charge point. Jabbari,
365 2015 demonstrated that, as the pH increases, a reduction of GA molecular charge is
366 observed, and its molecular charge is zero when the pH is about 6.0. This confirms that,
367 when the pH is close to 5.0, the GA is mostly protonated. Based on the previous
368 considerations, one can argue that adsorption of GA on the nanocomposites may occur
369 through two different mechanisms, on two different locations: i) the silanol groups
370 present on the surface of the nanocomposites; ii) the acidic Lewis sites. As far as the
371 adsorption on silanol groups present on the surface of the nanocomposites is concerned,
372 the pH range around 5.0 represents the only interval in which electrostatic repulsion
373 between the nanocomposites and GA is avoided. Thus, the main interactions occurring
374 between GA and the nanocomposites appear those based on physisorption mechanisms,
375 i.e. π - π interactions, Van der Waals forces, hydrophobic interactions (Zhang et al.,
376 2008). A significant reduction of the adsorption is observed at pH values higher than
377 6.0, similar to that recorded in previous studies on the adsorption of phenolic
378 compounds on zeolitic materials (Ahmat et al., 2019; Simon et al., 2015). This result
379 can be explained taking into account that the carboxylic acid moiety is completely
380 converted to carboxylate anion, and a significant amount of GA bears two negative
381 charges. These negative charges are stabilized in that the dissociation of orthophenolic
382 OH groups results in the formation of resonant structures, enhancing the conjugation of
383 the original polyphenol ring. Previous studies concerning the GA adsorption on various

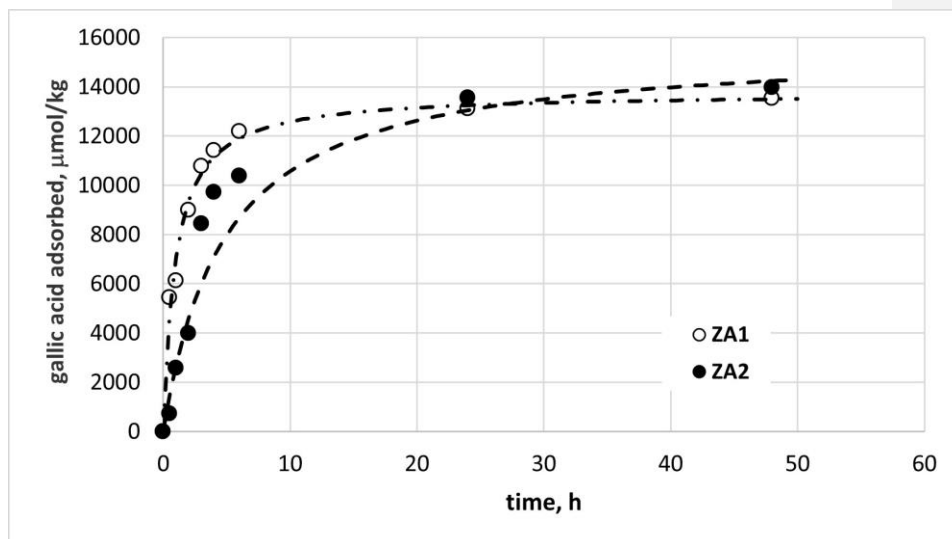
384 adsorbents (Ahmat et al., 2019; Celestino et al., 2019) also indicated the pH as a
385 fundamental factor in the adsorption phenomena due to its impact on both the surface
386 charge of the adsorbent and the ionisation of the adsorbate. In particular, although the
387 adsorbents tested were different, Celestino et al., 2019 observed the maximum
388 adsorption at pH 4-5. On the contrary, Ahmat et al., 2019 in a study focused on the
389 interactions of gallic acid with clay minerals, found that the adsorption was particularly
390 enhanced at pH 2.0 ($\approx 20,000 \mu\text{mol/kg}$). In order to explain this result, they made the
391 hypothesis that, at very low pH, the predominance of the protonated form of GA causes
392 a decrease of the repulsion between the neutral GA and Na-montmorillonite.
393 Contemporaneously, the electric charge of clay mineral surface turns cationic, favouring
394 the adsorption of phenolic acids in their anionic form. As under these conditions the GA
395 is almost completely protonated, these authors explained the maximum of GA
396 adsorption at pH = 2.0 with a possible cation exchange process. However, the amount of
397 GA adsorbed turns out to be much lower than that observed with the ZA1 and ZA2
398 samples, i.e. 70,000 and 60,000 $\mu\text{mol/kg}$, respectively (*vide infra*, adsorption
399 isotherms). As far as the adsorption on the acidic Lewis sites is concerned, the electron
400 lone pairs of the oxygen atoms of ionized carboxylic groups (about 25 % at pH = 5)
401 interact with the electron hole of the acidic Lewis sites, thus resulting in GA adsorption
402 on the surface of the nanocomposites. Obviously, the removal of ionized GA from water
403 by adsorption, promotes a further GA dissociation and, thus, the concentration of
404 negatively ionized GA molecules in solution remains about constant. Also this kind of
405 adsorption is depressed by pH different from 5.0. Actually: i) the amount of negatively
406 ionized GA is still lower at pHs lower than 5.0; ii) an higher hydroxyl anion
407 concentration preferentially saturates the acidic Lewis sites, being a stronger base than
408 negatively ionized GA molecules, at pHs higher than 5.0. Moreover, adsorption on the
409 acidic Lewis sites explains the higher extent to which adsorption occurs on ZA1
410 (bearing a far higher number of acidic Lewis sites) than on ZA2 (bearing a far lower
411 number of acidic Lewis sites).

412

413 3.3. Adsorption kinetic

414

415 The kinetics features of GA (148 $\mu\text{mol/L}$ initial added concentration) uptake from
 416 water by ZA1 and ZA2, (S/L ratio=1/100) at pH 5.0 are described in Figure 4.
 417



418
 419 **Figure 4.** Adsorption kinetics of gallic acid uptake on the magnetic adsorbents ZA1 and ZA2.
 420 S/L ratio = 1/100, pH 5.0, initial gallic acid concentration = 150 $\mu\text{mol/L}$.
 421

422 The experimental data show an initial sharp increase of the adsorbed amount,
 423 followed by a progressive slow down and, after about 24 h, an equilibrium condition.
 424 The initial adsorption rate (i.e. the slope of the linear portion of the curves) of ZA1 is
 425 faster in comparison to ZA2, (14,700 $\mu\text{mol}/(\text{kg h})$ and 2,350 $\mu\text{mol}/(\text{kg h})$, respectively)
 426 although the amounts of GA adsorbed at equilibrium are substantially similar. The
 427 asymptotic level reached after 24 h from the curves in Fig. 4 (about 13,000 $\mu\text{mol/kg}$)
 428 were considered as equilibrium values in the subsequent tests.

429 The experimental curves were best-fitted by the pseudo-second order kinetic
 430 model, that has been widely adopted for the adsorption of phenolic compounds in
 431 liquid-phase (Wu et al., 2009):

$$432 \quad \frac{t}{q_t} = \frac{1}{k_2 \cdot q_e^2} + \frac{t}{q_e} \quad (1)$$

433 where q_e and q_t are the sorption capacity (expressed in $\mu\text{mol/kg}$) at equilibrium
434 and at time t , respectively. The parameter k_2 , expressed in $\text{kg}/(\mu\text{mol min})$, is the overall
435 rate constant of pseudo second order sorption. The estimates of the parameters included
436 in the model (1), obtained by nonlinear regression, are reported in the Table 1.

437

438 **Table 1**

439 Estimates of the parameters included in the pseudo-second order model (1).

	ZA1	ZA2
$q_e, \mu\text{mol/kg}$	13,760	15,660
$k_2 \text{ kg}/\mu\text{mol min}$	1.07	0.208

440

441 Other authors showed that the adsorption kinetic of gallic acid onto magnetic ion
442 exchange resin (Ding et al., 2020) and on other adsorbents such as arginine-modified
443 magnetic chitosan (AMCS) (Chai et al., 2020), fitted well with the pseudo second-order
444 model.

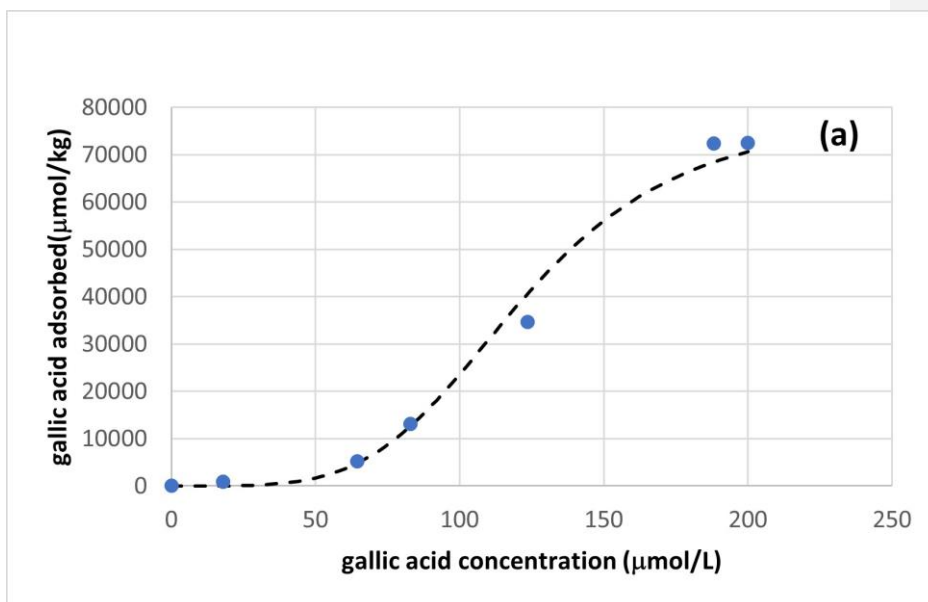
445

446 *3.4 Adsorption isotherms*

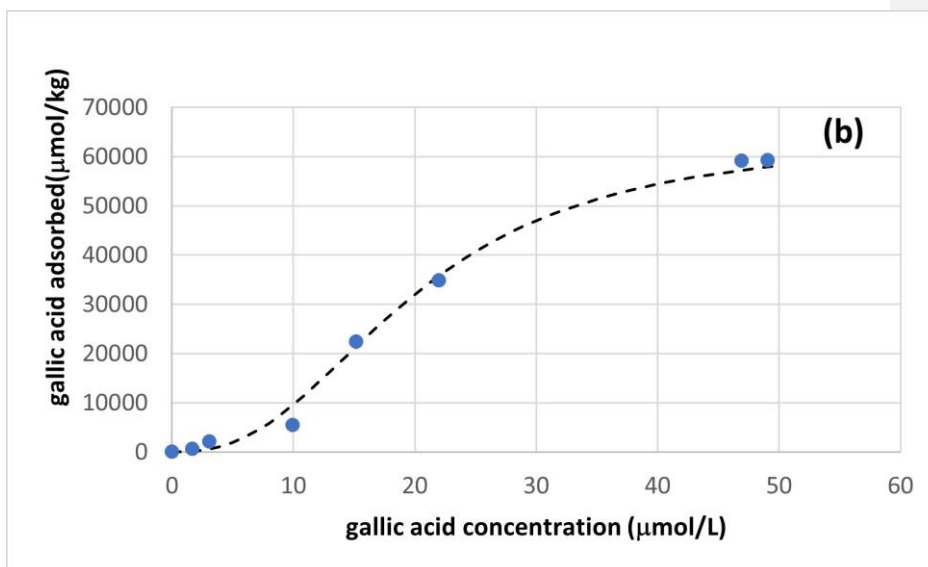
447

448 The adsorption isotherms for both the magnetic nanocomposites ZA1 and ZA2 are
449 reported in Figure 5 in terms of adsorbed amounts of each nanocomposite after a 24 h
450 incubation time as a function of GA concentration. The sigmoidal behaviour of the
451 curves shown by both materials suggests V type isotherms. Such isotherms are usually
452 adopted to describe the capillary condensation during the pore filling of micropores, and
453 cover the adsorption of water on hydrophobic microporous solids such as zeolite-
454 analogue materials (Kohler et al., 2017), as well as mesoporous materials.

455



456



457

458

459 **Figure 5.** Adsorption isotherms of gallic acid on the magnetic adsorbents ZA1 (a) and ZA2

460 (b).

461

462 The experimental curves have been fitted using the model of Sips, that has been
 463 previously adopted for the adsorption of phenolic compounds in liquid-phase (Leitão
 464 and Serrao, 2005; Carvajal-Bernal et al., 2017):

$$465 \quad q_t = \frac{q_m (K_s \cdot C_e)^{\frac{1}{m}}}{1 + (K_s \cdot C_e)^{\frac{1}{m}}} \quad (2)$$

466 where C_e is the equilibrium concentration of gallic acid, q_t is the sorption capacity
 467 of the zeolite (expressed in $\mu\text{mol/kg}$) at equilibrium. q_m ($\mu\text{mol/kg}$) is the maximum
 468 amount of GA adsorbed per unit mass of magnetic nanocomposite, K_s ($\text{L}/\mu\text{mol}$) is the
 469 Sips constant related to energy of adsorption, and the parameter m could be regarded as
 470 the parameter characterizing the system heterogeneity.

471 The Sips isotherm model is a combination of the Langmuir and Freundlich
 472 isotherm type models and expected to describe heterogeneous surface much better. At
 473 low adsorbate concentrations, the Sips isotherm approaches the Freundlich isotherm,
 474 whereas it approaches the Langmuir isotherm at high concentrations. The estimates of
 475 the parameters included in the model (2) are reported in the Table 2.

476

477 **Table 2**

478 Estimates of the parameters included in the Sips model (2).

	ZA1	ZA2
$q_m, \mu\text{mol/kg}$	79,100	64,200
$K_s, \text{L}/\mu\text{mol}$	0.0082	0.051
$m, -$	0.23	0.40

479

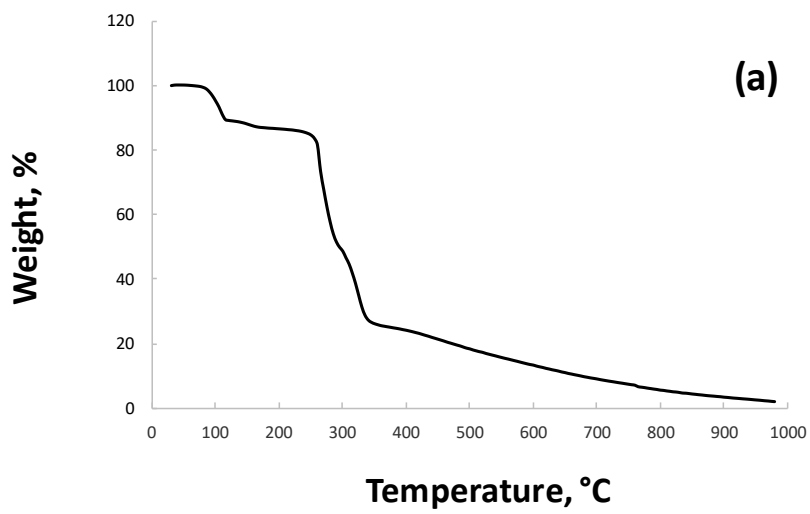
480 3.5 Desorption and recycle of the adsorbent

481

482 The regeneration and the reuse of the adsorbents play a crucial role in the
 483 economical balance of an adsorption process, as they can save resources improving the
 484 utilization efficiency. In this view, different desorption procedures were tested. First, to
 485 develop an efficient procedure for the thermal regeneration of the exhausted adsorbents,

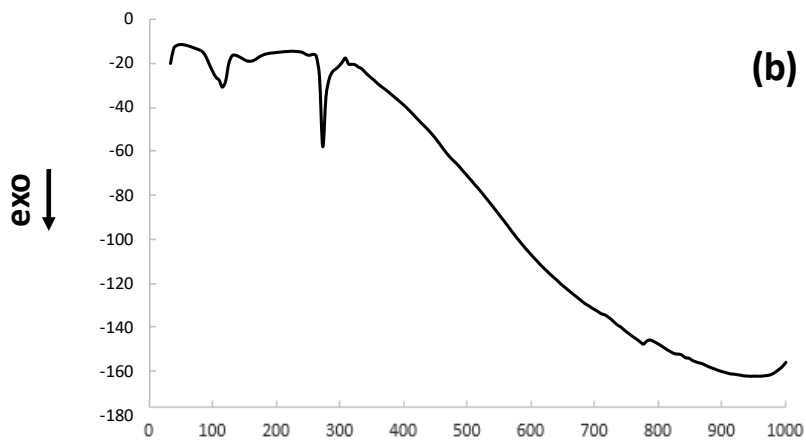
486 TGA and DTA analyses were carried on pure GA as well as on both ZA1 and ZA2
487 nanocomposites. The thermal analysis of GA (Figure 6a) showed a sharp endothermic
488 peak at about 270°C that can be reasonably ascribed to its thermal decomposition. This
489 hypothesis was confirmed by the TGA curve (Figure 6b), showing a sharp mass loss
490 (65% of the total) in the range 270-330°C.

491



492

493



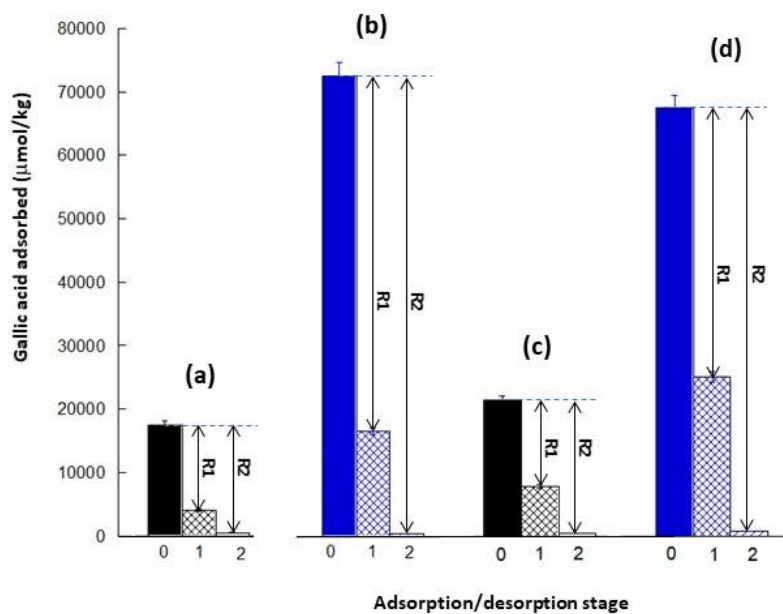
494

495 **Figure 6.** DTA curve (a) and TG curve (b) of gallic acid.

496

497 These results indicate that a thermal regeneration of the exhausted adsorbents can
498 be carried out by thermally treating the exhausted, GA bearing, adsorbents, at about
499 300°C under an inert atmosphere, to avoid the oxidation of Fe⁰ or Fe₃O₄ nanoparticles.
500 On the other hands, the TGA and DTA curves of ZA1 and ZA2 demonstrate high
501 thermal and chemical stability of the adsorbents at temperatures far higher than 300°C.
502 In order to find a more environmentally friendly strategy and to recover the GA, a
503 desorption procedure based on pH changes, as described in the Materials and Methods
504 section, was then attempted. The desorption procedure was fully unsuccessful at pH 5,
505 demonstrating that at this value of pH the adsorption equilibrium is completely shifted
506 towards the adsorbed phase (data not shown). On the contrary, when carrying out the
507 desorption at pH 8, the results were much more satisfactory. The results shown in the
508 Figure 7 demonstrate that a complete regeneration was obtained after the second
509 desorption cycle, whatever the initial concentration of GA adopted (200 µmol/L and
510 1000 µmol/L) and the nanocomposite used (ZA1 and ZA2). These results confirmed the
511 strong dependence of the adsorption of GA on ZA1 and ZA2 on pH, as previously
512 evidenced (*vide supra*).

513



514
 515 **Figure 7.** Regeneration of the exhausted adsorbent at pH 8 under different operating
 516 conditions:

517 (a): adsorbent ZA1, initial concentration: 200 µmol/L, pH 8

518 (b): adsorbent ZA1, initial concentration: 1000 µmol/L, pH 8

519 (c): adsorbent ZA2, initial concentration: 200 µmol/L, pH 8

520 (d): adsorbent ZA2, initial concentration: 1000 µmol/L, pH 8

521 Rectangles:

522 0 – gallic acid adsorbed before desorption

523 1 – residual GA adsorbed after the first desorption stage

524 2 – residual GA adsorbed after the second desorption stage

525 Arrows:

526 R1: Amount of GA released during the first desorption stage

527 R2: Amount of GA released during the first two desorption stages

528

529

530 **4. Conclusions**

531

532 The adsorption of GA, a toxic pollutant increasingly found in wastewaters from
533 food and pharmaceutical industries, has been efficiently carried out using two tailor-
534 made magnetic metal-ceramic nanocomposites, obtained from zeolite A (ZA1 and
535 ZA2). The nanocomposites have been developed by a cation-exchange treatment
536 followed by a thermal treatment at relatively moderate temperatures under reducing
537 atmosphere. The efficiency of the magnetic adsorbents strongly depends on pH, with a
538 maximum in the pH range around 5.0. In this interval the two different modalities of
539 GA adsorption on ZA1 and ZA2 attain their maximum for different reasons previously
540 explained.

541 The adsorption kinetics is described by the pseudo-second order model. The
542 equilibrium isotherms were satisfactorily described by the Sips model, a combination of
543 the Langmuir and Freundlich isotherm type models. Specific tests were carried out to
544 develop a procedure for the regeneration of exhausted adsorbents. First, a thermal
545 regeneration procedure was developed on the basis of the results of DT and TGA
546 analyses. In order to offer a more environmentally friendly, an alkaline desorption was
547 carried out, obtaining the complete regeneration of the magnetic adsorbents and recover
548 of GA. The results obtained demonstrate that magnetic metal-ceramic nanocomposites
549 obtained from zeolites offer a technically and economically feasible method to remove
550 GA from wastewaters, ensuring environmental sustainability, multicycle regenerability
551 of the adsorbents, and the recovery of the economically valuable product.

552

553 **CRedit authorship contribution statement**

554 **Domenico Pirozzi**: Data curation, Writing – original draft. **Michele Pansini**:
555 Writing/review and editing. **Antonello Marocco**: Investigation; Methodology. **Serena**
556 **Esposito**: Visualization, Writing - review & editing. **Gabriele Barrera**: Investigation;
557 Methodology. **Paola Tiberto**: Investigation; Methodology. **Paolo Allia**: Investigation;
558 Methodology. **Filomena Sannino**: Supervision, Writing – original draft.

559

560

561

562 **Declaration of Competing Interest**

563 The authors declare that they have no known competing financial interests or personal
564 relationships that could have appeared to influence the work reported in this paper.

565

566 **Funding:** This research received no external funding.

567

568

569

570

571

572

573

574

575

576

577

578

579

580

581

582

583

584

585

586

587

588

589

590

591

592

593

594

595

596

597

598

599

600

601

602 **References**

- 603
- 604 Addorisio, V., Esposito, S., Sannino, F., 2010. Sorption capacity of mesoporous metal
605 oxides for the removal of MCPA from polluted waters. *J. Agric. Food Chem.* 58,
606 5011-5016.
- 607 Addorisio, V., Pirozzi, D., Esposito, S., Sannino, F., 2011. Decontamination of waters
608 polluted with simazine by sorption on mesoporous metal oxides. *J. Hazard. Mater.*
609 196, 242-247.
- 610 Ahmat, A.M., Thiebault, T., Guégan, R., 2019. Phenolic acids interactions with clay
611 minerals: A spotlight on the adsorption mechanisms of gallic acid onto
612 montmorillonite. *Appl. Clay Sci.* 180, 105188,
613 <https://doi.org/10.1016/j.clay.2019.105188>.
- 614 Al Zahrani, N.A., El-Shishtawy, R.M., Asiri, A.M., 2020. Recent developments of
615 gallic acid derivatives and their hybrids in medicinal chemistry: A review. *Eur. J.*
616 *Med. Chem.* 204, 112609, <https://doi.org/10.1016/j.ejmech.2020.112609>.
- 617 Badhani, B., Sharma, N., Kakkar, R., 2015. Gallic acid: a versatile antioxidant with
618 promising therapeutic and industrial applications. *RSC Adv.* 5, 27540-27557,
619 <https://doi.org/10.1039/C5RA01911G>.
- 620 Carvajal-Bernal, A.M., Gomez-Granados, F., Giraldo, L., Moreno-Pirajan, J.C., 2017.
621 Application of the Sips model to the calculation of maximum adsorption capacity
622 and immersion enthalpy of phenol aqueous solutions on activated carbons. *Chem.*
623 *Eur. J.* 8, 112-118.
- 624 Celestino, G.G., Henriques, R.R., Shiguihara, A.L., Constantino, V.R.L., de Siqueira
625 Melo, R., Amim Júnior, J., 2019. Adsorption of gallic acid on nanoclay modified
626 with poly(diallyldimethylammonium chloride). *Environ. Sci. Pollut. Res. Int.*,
627 26(28), 28444-28454.
- 628 Chai, Z., Li, C., Zhu, Y., Song, X., Chen, M., Yang, Y., Chen, D., Liang, X., Wu, J.,
629 2020. Arginine-modified magnetic chitosan: Preparation, characterization and
630 adsorption of gallic acid in sugar solution. *Int. J. Biol. Macromol.* 165, 506-516.
- 631 Clayden, E., Esposito, S., Ferone, C., Pansini, M., 2003. ²⁷Al and ²⁸Si NMR study of the
632 thermal transformation of Ba-exchanged zeolite A into monoclinic celsian. *J. Mat.*
633 *Chem.* 13, 1681-1685.
- 634 Colantuono, A., Dal Vecchio, S., Mascolo, G., Pansini, M., 1997. Thermal shrinkage of
635 various cation forms of zeolite A. *Thermochim. Acta* 296, 59-66.
- 636 Di Martino, M., Sannino, F., Pirozzi, D., 2015. Removal of pesticide from wastewater:
637 Contact time optimization for a two-stage batch stirred adsorber. *J. Environ.*
638 *Chem. Eng.* 3, 365-372.
- 639 Ding, L., Guo, C., Zhu, Y., Ma, J., Kong, Y., Zhong, M., Cao, Q., Zhang, H., 2020.
640 Adsorptive removal of gallic acid from aqueous solution onto magnetic ion
641 exchange resin. *Water Sci. Technol.* 81, 1479-1493.
- 642 Esposito, S., Dell'Agli, G., Marocco, A., Bonelli, B., Allia, P., Tiberto, P., Barrera, G.,
643 Manzoli, M., Arletti, R., Pansini, M., 2018. Magnetic metal-ceramic
644 nanocomposites obtained from cation-exchanged zeolite by heat treatment in
645 reducing atmosphere. *Microporous Mesoporous Mater.* 268, 131-143.
- 646 Esposito, S., Marocco, A., Bonelli, B., Pansini, M., 2015. PCT international application
647 published under Number WO2015/145230 A1.
- 648 Esposito, S., Marocco, A., Dell'Agli, G., Bonelli, B., Mannu, F., Allia, P., Tiberto, P.,
649 Barrera, G., Pansini, M., 2020. Separation of biological entities from human blood

650 by using magnetic nanocomposites obtained from zeolite precursors. *Molecules*
651 25, 1803-1820 [https://doi:10.3390/molecules25081803](https://doi.org/10.3390/molecules25081803).
652 Esposito, S., Pansini, M., Bonelli, B., Garrone, E., 2013. Modes of interaction of
653 simazine with the surface of model amorphous silica in water. *J. Phys. Chem.* 117
654 (21), 11203-11210.
655 Freyria, F.S., Marocco, A., Esposito, S., Bonelli, B., Barrera, G., Tiberto, P., Allia, P.,
656 Oudayer, P., Roggero, A., Matéo-Vélez, J.C., Dantras, E., Pansini, M., 2019.
657 Simulated moon agglutinates obtained from zeolite precursor by means of a low-
658 cost and scalable synthesis method. *ACS Earth Sp. Chem.* 3 (9), 1884-1895.
659 Friedman, M., Jürgens, H.S., 2000. Effect of pH on the stability of plant phenolic
660 compounds. *J. Agric. Food Chem.* 48, 2101-2110.
661 Guo, F.Q., Li, X.L., Jiang, X.C., Zhao, X.M., Guo, C.L., Rao, Z.H., 2018.
662 Characteristics and toxic dye adsorption of magnetic activated carbon prepared
663 from biomass waste by modified one-step synthesis. *Colloids Surf. A*
664 *Physicochem. Eng. Asp.* 555, 43-54.
665 Hirun, N., Dokmaisrijan, S., Tantishaiyakul, V., 2012. Experimental FTIR and
666 theoretical studies of gallic acid-acetonitrile clusters. *Spectrochim. Acta A* 86, 93-
667 100.
668 Hsieh, C.L., Lin, C.H., Wang, H.E., Peng, C.C., Peng, R.Y., 2015. Gallic acid exhibits
669 risks of inducing muscular hemorrhagic liposis and cerebral hemorrhage—its
670 action mechanism and preventive strategy. *Phytother. Res.* 29, 267-280.
671 Jabbari, M., 2015. Solvent dependence of protonation equilibria for gallic acid in water
672 and different acetonitrile-water cosolvent systems. *J. Mol. Liq.* 208, 5-10.
673 Kohler, T., Hinze, M., Müller, K., Schwieger, W., 2017. Temperature independent
674 description of water adsorption on zeo-types showing a type V adsorption
675 isotherm. *Energy* 135, 227-236.
676 Leitão, A., Serrão, R., 2005. Adsorption of phenolic compounds from water on
677 activated carbon: prediction of multicomponent equilibrium isotherms using
678 single-component data. *Adsorption* 11, 167-179.
679 Lu, Z.B., Nie, G.J., Belton, P.S., Tang, H.R., Zhao, B.L., 2006. Structure-activity
680 relationship analysis of antioxidant ability and neuroprotective effect of gallic acid
681 derivatives. *Neurochem. Int.* 48, 263-274.
682 Manzoli, M., Tamaro, O., Marocco, A., Bonelli, B., Barrera, G., Tiberto, P., Allia, P.,
683 Matéo-Vélez, J.C., Roggero, A., Dantras, E., Arletti, R., Pansini, M., Esposito, S.,
684 2021. New insight in the production of simulated moon agglutinates: the use of
685 natural zeolite-bearing rocks. *ACS Earth Sp. Chem.* 5 (6), 1631-1646.
686 Marocco, A., Dell'Agli, G., Pansini, M., Sannino, F., Allia, P., Tiberto, P., Barrera, G.,
687 Esposito, S., 2019. Removal of agrochemicals from water by adsorption: a
688 critical comparison among humic-like substances, zeolites, porous oxides, and
689 magnetic nanocomposites. *Processes* 8, 141-167.
690 Marocco, A., Liguori, B., Dell'Agli, G., Bonelli, B., Pansini, M., 2011. Sintering
691 behavior of celsian based ceramics obtained from the thermal transformation of
692 Ba-exchanged zeolite A into monoclinic celsian. *J. Eur. Ceram. Soc.* 31, 1965-
693 1973.
694 Moreno-Álvarez, S.A., Martínez-Castañón, G.A., Niño-Martínez, N., Reyes-Macías,
695 J.F., Patiño-Marín, N., Loyola-Rodríguez, J.P., Ruiz, F., 2010. Preparation and
696 bactericide activity of gallic acid stabilized gold nanoparticles. *J. Nanopart. Res.*
697 12, 2741-2746.

Commentato [ES1]: Non è un inizio pagina ma un numero
identificativo

- 698 Pansini, M., Dell'Agli, G., Marocco, A., Netti, P.A., Battista, E., Lettera, V., Vergara,
699 P., Allia, P., Bonelli, B., Tiberto, P., Barrera, G., Martra, G., Arletti, R., Esposito,
700 S., 2017. Preparation and characterization of porous metal-ceramic
701 nanocomposites from a zeolite precursor and their application for DNA
702 separation. *J. Biomed. Nanotechnol.* 13 (3), 337-348.
- 703 Pansini M., Sannino, F., Marocco, A., Allia, P.M., Tiberto, P., Barrera, G., Polisi, M.,
704 Battista, E., Netti, P., Esposito, S., 2018. Novel process to prepare magnetic
705 metal-ceramic nanocomposites from zeolite precursor and their use as adsorbent
706 of agrochemicals from water. *J. Environ. Chem. Eng.* 6 (1), 527-538.
- 707 Pant, A.F., Özkasikci, D., Fürtauer, S., Reinelt, M., 2019. The effect of deprotonation
708 on the reaction kinetics of an oxygen scavenger based on gallic acid. *Front. Chem.*
709 7, 680-686.
- 710 Pasanphan, W., Buettner, G.R., Chirachanchai, S., 2010. Chitosan gallate as a novel
711 potential polysaccharide antioxidant: an EPR study. *Carbohydr. Res.* 345, 132-
712 140.
- 713 Pirozzi D., Sannino F., 2014. Design of a multi-stage stirred adsorber using mesoporous
714 metal oxides for herbicide removal from wastewaters. *J. Environ. Chem. Eng.* 2,
715 211-219.
- 716 Sannino, F., Pansini, M., Marocco, A., Cinquegrana, A., Esposito, S., Tammaro, O.,
717 Barrera, G., Tiberto, P., Allia, P., Pirozzi, D., 2022. Removal of sulfanilamide by
718 tailor-made metal-ceramic nanocomposite adsorbents. *J. Environ. Manag.* 310,
719 114701-114709.
- 720 Sannino, F., Ruocco, S., Marocco, A., Esposito, S., Pansini, M., 2012. [Cyclic process of
721 simazine removal from waters by adsorption on zeolite H-Y and its regeneration
722 by thermal treatment](#)~~Simazine removal from waters by adsorption on zeolite H-Y
723 and its regeneration by thermal treatment~~. *J. Hazard. Mat.* 229-230, 354-360.
- 724 Sannino, F., Ruocco, S., Marocco, A., Esposito, S., Pansini, M., 2013. Simazine
725 removal from waters by adsorption on porous silica tailored by the sol-gel
726 technique. *Micr. Mes. Mat.* 180, 178-186.
- 727 Simon, V., Thuret, A., Candy, L., Bassil, S., Duthen, S., Raynaud, C., Masseron, A.,
728 2015. Recovery of hydroxycinnamic acids from renewable resources by adsorption
729 on zeolites, *Chem. Eng. J.* 280, 748-754.
- 730 Sousa, A.M.L., Li, T.D., Varghese, S., Halling, P.J., Lau, K.H.A., 2018. Highly active
731 protein surfaces enabled by plant-based polyphenol coatings. *ACS Appl. Mater.*
732 *Interfaces* 10, 39353-39362.
- 733 Srivastava, B., Jhelum, V., Basu, D.D., Patanjali, P.K. 2009. Adsorbents for pesticide
734 uptake from contaminated water: a review. *J. Sci. Ind. Res.* 68, 839-850.
- 735 Wan, J., Ding, J., Tan, W., Gao, Y., Sun, S., He, C., 2020. Magnetic-activated carbon
736 composites derived from iron sludge and biological sludge for sulfonamide
737 antibiotic removal. *Environ. Sci. Poll. Res.* 27, 13436-13446.
- 738 Weidentaler, C., Zibrovius, B., Schimanke, J., Mao, Y., Mienert, B., Schmidt, W., 2005.
739 Behavior of ferrous cations during ion exchange into zeolites under atmospheric
740 conditions. *Micr. Mes. Mat.* 84, 302-317.
- 741 Wu, F.C., Tseng, R.L., Huang, S.C., Juang, R.S., 2009. Characteristics of pseudo-
742 second-order kinetic model for liquid-phase adsorption: A mini-review. *Chem.*
743 *Eng. J.* 151, 1-9.
- 744 Yang, W., Ding, H., Qi, G., Li, C., Xu, P., Zheng, T., Zhu, X., Kenny, J.M., Puglia, D.,
745 Ma, P., 2021. Highly transparent PVA/nanolignin composite films with excellent

Commentato [ES2]: Non è un inizio pagina ma un numero identificativo

746 UV shielding, antibacterial and antioxidant performance. *React. Funct. Polym.*
747 162, 104873-104882.
748 Zhang, Y., Dong, L., Li, J., Chen, X., 2008. Studies on the interaction of gallic acid with
749 human serum albumin in membrane mimetic environments. *Talanta*, 76, 246-253.
750 Zhang, Z, Pang, Q, Li, M, Zheng, H, Chen, H, Chen, K, 2015. Optimization of the
751 condition for adsorption of gallic acid by *Aspergillus oryzae* mycelia using Box-
752 Behnken design. *Environ Sci Pollut Res*, 22, 1085-1094.
753 Zheng, M., Zhang, C., Zhou, Y., Lu, Z., Zhao, H., Bie, X., Lu, F., 2018. Preparation of
754 gallic acid-grafted chitosan using recombinant bacterial laccase and its application
755 in chilled meat preservation. *Front. Microbiol.* 9, 1729-1738.
756
757